JOURNAL OF GEOPHYSICAL RESEARCH, VOL. 101, NO. D22, PAGES 29,305–29,316, DECEMBER 20, 1996

Three-dimensional view of the large-scale tropospheric ozone distribution over the North Atlantic Ocean during summer

P. Kasibhatla,[1,2] H. Levy II,[3] A. Klonecki,[4] and W. L. Chameides[1]

Abstract. A global chemical transport model is used to study the three-dimensional structure of the tropospheric ozone (O_3) distribution over the North Atlantic Ocean during summer. A simplified representation of summertime O_3 photochemistry appropriate for northern hemisphere midlatitudes is included in the model. The model is evaluated by comparing simulated O_3 mixing ratios to summertime O_3 measurements taken in and near the North Atlantic Ocean basin. The model successfully reproduces (1) the means and standard deviations of ozonesonde measurements over North America at 500 mbar; (2) the statistical characteristics of surface O_3 data at Sable Island off the coast of North America and at Bermuda in the western North Atlantic; and (3) the mean midtropospheric O_3 measured at Bermuda and also at the Azores in the eastern North Atlantic. The model underestimates surface O_3 in the eastern North Atlantic, overestimates O_3 in the lower free troposphere over the western North Atlantic, and also has difficulty simulating the upper tropospheric ozonesonde measurements over North America. An examination of the mean summertime O_3 distribution simulated by the model shows a significant continental influence on boundary layer and free-tropospheric O_3 over the western North Atlantic. The model has also been exercised using a preindustrial NO_x emission scenario. By comparing the present-day and preindustrial simulations, we conclude that anthropogenic NO_x emissions have significantly perturbed tropospheric O_3 levels over most of the North Atlantic. We estimate that present-day O_3 levels in the lower troposphere over the North Atlantic are at least twice as high as corresponding preindustrial O_3 levels. We find that the anthropogenic impact is substantial even in the midtroposphere, where modeled present-day O_3 mixing ratios are at least 1.5 times higher than preindustrial O_3 levels.

1. Introduction

Tropospheric ozone (O_3) plays a central role in determining the oxidizing capacity of the troposphere [*Levy*, 1971], and is also an important greenhouse gas [*Manabe and Strickler*, 1964; *Manabe and Wetherald*, 1967; *Ramanathan et al.*, 1985]. A detailed assessment of the global tropospheric O_3 budget is therefore important not only from an atmospheric chemistry perspective but also from a climate and global change perspective. The two sources of tropospheric O_3 are downward transport from the stratosphere [e.g., *Junge*, 1962; *Chatfield and Harrison*, 1977; *Mahlman et al.*, 1980; *Levy et al.*, 1985] and photochemical production in the troposphere itself by reactions involving precursor nitrogen oxides (NO_x = NO + NO_2), carbon monoxide (CO), methane, and nonmethane hydrocarbons [*Chameides and Walker*, 1973; *Crutzen*, 1974]. However, considerable uncertainty persists in our understanding of the relative importance of these two sources, especially in marine regions where both transport and chemistry can play important roles in shaping the ozone budget [e.g., *Levy et al.*, 1985].

One region of particular interest in terms of human impacts on tropospheric chemistry is the North Atlantic Ocean (NAO) basin. Bordered by the industrialized continental regions of North America and Europe, where significant emissions of O_3-precursor gases occur, the NAO is where one would likely find the strongest signature of the anthropogenic influence on marine tropospheric O_3. Indeed, there is observational and theoretical evidence suggesting that significant amounts of photochemically generated O_3 are exported from the continental source regions to the NAO during summer [*Harriss et al.*, 1984; *Winkler*, 1988; *Fishman et al.*, 1990; *Parrish et al.*, 1993; *Jacob et al.*, 1993b]. However, there is also observational and theoretical evidence that seems to suggest that surface O_3 over the North Atlantic is predominantly natural in origin during much of the year [*Levy et al.*, 1985; *Oltmans and Levy*, 1992].

Numerical chemical transport models (CTMs) provide powerful tools with which to study this problem. Three-dimensional episodic models have yielded useful insights into the behavior of tropospheric ozone on continental and intercontinental scales [*Brost et al.*, 1988; *McKeen et al.*, 1991; *Mathur et al.*, 1994]. From a global and climatological perspective, most previous modeling studies of tropospheric O_3 chemistry have relied on one- and two-dimensional models [e.g., *Crutzen and Gidel*, 1983; *Isaksen and Hov*, 1987; *Hough and Derwent*, 1990; *Lu and Khalil*, 1991; *Pinto and Khalil*, 1991; *Law and Pyle*, 1991; *Thompson et al.*, 1993]. These lower-dimensional models suffer from the drawback that they cannot capture the complex in-

[1]School of Earth and Atmospheric Sciences, Georgia Institute of Technology, Atlanta.
[2]Now at Environmental Programs, MCNC, Research Triangle Park, North Carolina.
[3]NOAA Geophysical Fluid Dynamics Laboratory, Princeton, New Jersey.
[4]Atmospheric and Ocean Sciences Program, Princeton University, Princeton, New Jersey.

Paper number 95JD03234.
0148-0227/96/95JD-03234$09.00

teraction among transport, chemistry, and a geographically inhomogeneous physical source-sink distribution, particularly for short-lived O_3-precursor gases such as NO_x [*World Meteorological Organization (WMO)*, 1994]. *Crutzen and Zimmerman* [1991] have used a global, three-dimensional CTM to simulate present and preindustrial O_3 distributions and concluded that human activities have significantly perturbed background O_3 concentrations, especially in the northern hemisphere (NH). However, their CTM is driven by monthly mean meteorological fields and thus does not simulate synoptic-scale meteorological features which are important elements of tracer transport [e.g., *Moxim*, 1990]. Furthermore, their model cannot simulate important aspects of summertime O_3 at NH midlatitudes, such as the occurrence of regional episodes of elevated O_3 in association with weak, stagnant anticyclones over the eastern United States [e.g., *Altshuller*, 1978; *Jacob et al.*, 1993a].

In this study we use a three-dimensional global chemical transport model (GCTM), which is driven by time-varying meteorological fields, to simulate the present-day summertime O_3 distribution over the entire NAO basin. While the treatment of transport processes is more realistic than in previous models of global O_3, only a simplified representation of tropospheric O_3 photochemistry is included in our model. In the following sections we describe various components of the GCTM used in this study, evaluate model performance by comparing model results at specific location to observations, and discuss the three-dimensional structure of the simulated large-scale summertime O_3 distribution over the NAO.

2. Model Description

The GCTM used in this study was developed at the Geophysical Fluid Dynamics Laboratory (GFDL) [*Mahlman and Moxim*, 1978; *Levy et al.*, 1982, 1985; *Levy and Moxim*, 1989]. In recent years the GCTM has been applied to study the cycling of reactive nitrogen compounds in the troposphere, in a joint effort between the Georgia Institute of Technology and the GFDL [*Kasibhatla et al.*, 1991, 1993; *Levy et al.*, 1991, 1993, 1995; *Kasibhatla*, 1993; *Galloway et al.*, 1994; *Moxim et al.*, 1995]. The model has a horizontal resolution of ~265 km and 11 sigma levels in the vertical at standard pressures of 10, 38, 65, 110, 190, 315, 500, 685, 835, 940, and 990 mbar. The model is driven using 12 months of 6-hour time-averaged meteorological fields from a GFDL general circulation model [*Manabe et al.*, 1974; *Manabe and Holloway*, 1975]. The basic structure of the GCTM and the calculation of tracer advection has been described by *Mahlman and Moxim* [1978]. The GCTM includes parameterized sub-grid-scale horizontal transport as well as vertical mixing by dry and moist convection. Details of these parameterizations can be found in the works of *Levy et al.* [1982], *Levy and Moxim* [1989], and *Kasibhatla et al.* [1993].

In the current application of the model, surface dry deposition rates of O_3 are calculated using a drag-coefficient formulation for surface exchange [*Levy and Moxim*, 1989], which is consistent with the treatment of this process in the parent general circulation model. Monthly and spatially varying dry deposition velocities are calculated using a standard resistance-in series model [*Wesely and Hicks*, 1977; *Wesely*, 1989], in conjunction with a $1^\circ \times 1^\circ$ map of land use data [*Mathews*, 1983]. The natural source of tropospheric O_3, due to downward transport from the stratosphere, is simulated by adjusting the O_3 mixing ratios at the top model level (10 mbar) to prescribed climatological monthly and latitudinally varying values [*Nagatani et al.*, 1988]. In this preliminary study, no chemistry is included in the lower stratosphere. Previous studies suggest that the transport biases in the GCTM tend to compensate for the missing lower-stratospheric chemistry [*Levy et al.*, 1985]. Some aspects of stratosphere-troposphere exchange in the model are also discussed by *Mahlman and Moxim* [1978] and *Mahlman et al.* [1980].

An accurate simulation of oxidant chemistry in the continental boundary layer is difficult due to uncertainties in reaction mechanisms and rates. An additional factor that must be considered is the computational expense involved in performing a detailed simulation of this chemistry. In this study, an alternative approach is used. Results from our previous studies of reactive nitrogen (NO_y) chemistry, along with observed empirical relationships between NO_y compounds and O_3, are used to simulate boundary layer O_3 photochemistry during summer at NH midlatitudes. This simplified boundary layer photochemical scheme is applied only in the bottom three model levels at 835, 940, and 990 mbar and is described in more detail below.

We first assume that boundary layer O_3 photochemistry is controlled by the ambient NO_x concentration, which is a reasonable assumption at NH midlatitudes during summer [*Chameides et al.*, 1992]. When the NO_x concentration at a model grid point at a particular time is less than a prescribed "NO_x balance point," photochemical processes are assumed to provide a net O_3 sink at a rate given by the sum of the $O_3 + h\nu \rightarrow O(^1D) + O_2$ and $(O^1D) + H_2O \rightarrow 2OH$ reactions. When the NO_x concentration at a model grid point is greater than the NO_x balance point, photochemical processes are assumed to provide a net source, and the rate of O_3 production is assumed to be proportional to the rate of NO_x oxidation. The NO_x balance point is set equal to 50 parts per trillion by volume (pptv) based on chemical box model calculations. In these box-model calculations, concentrations of O_3, methane, CO, and water vapor are fixed at values characteristic of the marine boundary layer over the NAO. Sensitivity calculations indicate that our model results are relatively insensitive to realistic changes in the NO_x balance point. For example, decreasing the NO_x balance point to 30 pptv resulted in at most a 10% change in calculated boundary layer O_3 mixing ratios over the NAO. The oxidation rates and mixing ratios of NO_x at each model grid point are taken from our previous simulations of NO_y compounds using the same GCTM (see Appendix) and are updated every six hours.

A key parameter in our boundary layer O_3 photochemical scheme is the yield of O_3 molecules per NO_x molecule oxidized. *Trainer et al.* [1993] analyzed measurements of O_3, NO_x, and NO_y from rural sites in North America and found a significant correlation between O_3 and the products of NO_x oxidation, i.e., (NO_y-NO_x). Furthermore, they suggested that this linear relationship was driven by the rapid oxidation of NO_x, with concomitant photochemical production of O_3, and that the slope of the linear regression line between O_3 and (NO_y-NO_x) can be interpreted as the effective yield of O_3 per NO_x molecule oxidized. *Trainer et al.* [1993] have also pointed out that a number of factors such as the ambient concentration of reactive hydrocarbons, the heterogeneous nighttime conversion of nitrogen pentoxide to nitric acid (HNO_3) without concomitant O_3 production, and the faster rate of HNO_3 dry deposition relative to O_3 can affect the relationship between O_3 and (NO_y-NO_x). Observations in the eastern United States and Europe indicate that the slope of O_3/(NO_y-NO_x) regres-

sion line generally ranges from 5 to 12 during summer [*Wang*, 1992; *Trainer et al.*, 1993; *Volz-Thomas et al.*, 1993]. *Jacob et al.* [1993b] calculated net O_3 production efficiencies (defined as the net rate of O_3 photochemical production divided by net rate of NO_x oxidation) ranging from 4.4 in the eastern United States to 12.4 in the western United States during summer in their three-dimensional model study of tropospheric O_3 over North America. The higher O_3 net production efficiency in the west is due to the increased O_3 photochemical production efficiency at lower NO_x concentrations [*Liu et al.*, 1987; *Lin et al.*, 1988]. An independent estimate of the net O_3 production efficiency can also be obtained by scaling observed O_3/CO ratios in a region by the CO/NO_x emission ratio in the same region [*Chin et al.*, 1994]. Applying this method to the eastern United States gives a net O_3 production efficiency of about 2.1 (D. J. Jacob and J. A. Logan, private communication), which must be viewed as a lower limit [*Chin et al.*, 1994].

In this study we assume that the net rate of O_3 photochemical production is proportional to the rate at which NO_x molecules are oxidized to HNO_3 by reaction with hydroxyl radicals (OH). We also assume that the yield of O_3 molecules per NO_x molecule oxidized is a constant, which is taken to be 8.5 based on the *Trainer et al.* [1992] study. Clearly, the assumption of a constant yield is a simplification. However, it should be noted that our focus is not on a detailed description of the O_3 distribution over the continental source regions but rather on the distribution of O_3 over the NAO. It should also be emphasized that our definition of the net O_3 photochemical yield is based only on the oxidation rate of NO_x by OH and is somewhat different than the *Jacob et al.* [1993b] definition which is based on the total NO_x oxidation rate, including heterogeneous nighttime HNO_3 production.

A simplified treatment of O_3 photochemistry in the free troposphere is also included in the model. This is done by specifying summer-mean (June–July–August mean) net O_3 photochemical tendencies (O_3 photochemical production rate—O_3 photochemical destruction rate) at each model grid point at the 315-, 500-, and 685-mbar model levels. The specification of the net O_3 photochemical tendency in each grid box at these altitudes is based on chemical box model calculations using climatological water vapor and temperature data [*Oort*, 1983], representative concentrations of methane (1.7 parts per million by volume (ppmv)) and CO (100–120 parts per billion by volume (ppbv)), summer-mean NO_x mixing ratios from our previous modeling studies (see Appendix), and summer-mean O_3 data generated by first running the GCTM without any free-tropospheric O_3 photochemistry. The calculated, net free-tropospheric O_3 photochemical tendencies used in this study are shown in Figure 1 for a subset of the global model domain. Net photochemical O_3 production is calculated to occur in the lower free troposphere over Europe and all the way up to 315 mbar over the eastern United States. Because of the presence of a significant free-tropospheric source of lightning-generated NO_x over the south central and southeastern United States in the model, the calculated free-tropospheric O_3 production rates in this region are higher than the corresponding production rates over Europe. Net O_3 photochemical destruction, ranging from 1 to 3 ppbv/d, is calculated to occur in the lower free troposphere over most of the NAO, while weak net O_3 photochemical production is calculated to occur downwind of North America and also south of 40°–45°N at the 315-mbar model level.

Given the simplified representation of tropospheric O_3 photochemistry in the model, it should be emphasized that our study is preliminary in nature. Nevertheless, the model captures the essence of the coupling between tropospheric chemistry and transport processes and can therefore provide useful insights into the three-dimensional structure of the tropospheric O_3 distribution over the NAO.

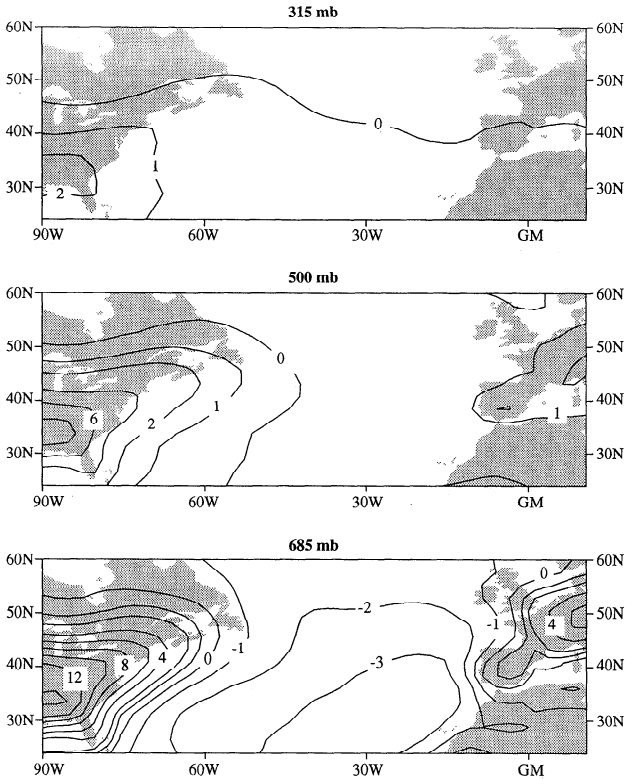

Figure 1. Free-tropospheric net O_3 photochemical tendencies used in the model at the 315-, 500-, and 685-mbar model levels. Contour levels are −3, −2, −1, 0, 1, 2, 4, 6, 8, 10, 12, and 14 ppbv O_3/d.

3. Discussion of Model Results

The GCTM described in the previous section has been used to simulate the distribution of O_3 over the entire global model domain. Since the simplified representation of tropospheric O_3 chemistry in the model is specifically designed to simulate summertime O_3 chemistry over the NH midlatitudes, we will focus our attention on an analysis of model results over the NAO and adjacent continents during summer only (July–August unless otherwise noted). We first compare model results to measurements at specific sites relevant to this study and then discuss the simulated large-scale tropospheric O_3 distribution over the NAO.

3.1. Comparisons With Measurements at Continental Locations

Since our model is driven by meteorological fields from one year of a general circulation model simulation, the most appropriate comparison of model results to measurements is a climatological one, preferably at locations where statistics from multiple-year measurements are available. We first focus on a comparison of model results with measurements over continental regions. In the continental boundary layer, a direct comparison of modeled and observed O_3 mixing ratios is prob-

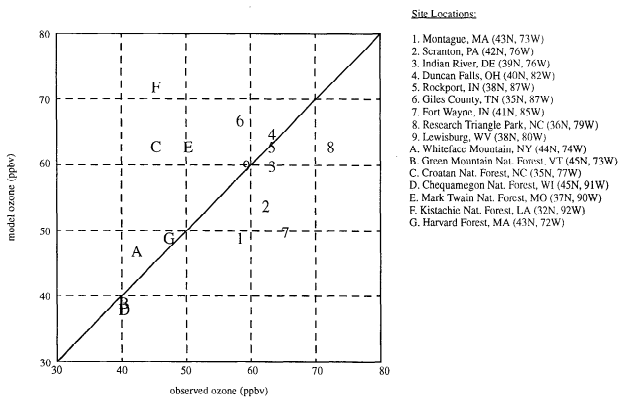

Figure 2. Comparison of median boundary layer average model O_3 mixing ratios with median afternoon surface O_3 concentrations measured at selected sites in the eastern United States during June–July–August. The observed values are listed by *Jacob et al.* [1993a, Table 4a], where references to the original data can also be found. Note that site J in the Jacob et al. paper corresponds to site G in this figure.

lematic due to sub-grid-scale spatial variability in O_3 concentrations and due to diurnal variations in boundary layer depth and O_3 photochemistry that our diurnally averaged model does not capture. Nevertheless, we have performed a limited comparison of boundary layer average model results with the median observed afternoon O_3 concentrations at the 16 rural sites east of 100°W in the United States used by *Jacob et al.* [1993a] to evaluate their model; this comparison is shown in Figure 2.

In a manner similar to the *Jacob et al.* [1993a] study, our model reproduces the large-scale contrast between high O_3 mixing ratios at sites along the Ohio River valley and low mixing ratios at sites removed from the population centers of the eastern United States. However, certain smaller-scale features are not reproduced due to the model grid resolution. For example, there is a 11 ppbv difference in the observed O_3 concentrations at sites 1 and G which the model is unable to resolve, since both sites lie in the same grid box in our model. Similarly, the model is unable to resolve the observed gradient between sites 8 and C, which lie in adjacent model grid boxes. On the other hand, at site 7 (where the model underpredicts O_3 by 15 ppbv) there is a large gradient in modeled O_3, with values of 57 and 65 ppbv present in model boxes to the west and east of this particular site. The overprediction at sites E and F is similar to that found by *Jacob et al.* [1993a] in their model, who suggest that this may be due to an excessive dilution of emissions from NO_x point sources in the south central United States, or due to an insufficient influx of maritime air from the Gulf of Mexico into this region.

We next compare simulated free-tropospheric mixing ratios with long-term ozonesonde measurements over North America and Europe. The data set used is the one compiled by *Logan* [1994] for Wallops Island (38°N, 76°W), Boulder (40°N, 105°W), Hohenpeissenberg (48°N, 11°E), Goose Bay (53°N, 60°W), Edmonton (53°N, 114°W), Churchill (59°N, 94°W), and Resolute (75°N, 95°W), supplemented by ozonesonde data from Haute Provence (44°N, 6°E) [*Beekmann et al.*, 1994]. Figure 3 shows a comparison of observed and modeled July–August mean O_3 mixing ratios and standard deviations at these sites (except at Haute Provence where only July-mean mixing ratios are available) from 750 to 150 mbar (where diurnal effects are probably less important). In the upper troposphere near the 300-mbar pressure level, the modeled mean O_3 levels at Wallops Island, Edmonton, and Churchill deviate from observations by about 25%, and the model standard deviations at Goose Bay, Churchill, and Resolute are significantly lower than the standard deviations in the observations. At this altitude, the model agrees well with the measurements at Hohenpeissenberg but does not reproduce the somewhat lower values of O_3 observed at Haute Provence. These discrepancies in the upper troposphere may be related to deficiencies in stratosphere-troposphere exchange in the model, but at this altitude the model results are also greatly affected by errors in the location of the local tropopause height in the model. The model also has difficulty is simulating the gradient in the vertical O_3 profile between the troposphere and the lower stratosphere at many of the sites. However, it is encouraging to note that these deficiencies do not seem to adversely affect model performance in the middle troposphere. The simulated O_3 mixing ratios at 500 mbar agree with observations to within about 15%; and the modeled standard deviations are also in good agreement with the corresponding observed statistics. It is also interesting to note that the model captures the variability in the 500-mbar data despite the lack of temporal variability in the free-tropospheric O_3 photochemical tendencies used in the model, suggesting that the variability in O_3 mixing ratios at this altitude is controlled by transport rather than by chemistry. Lower down in the free troposphere at around 700 mbar, the model overestimates the amount of O_3 at Wallops Island. This is likely related to an overestimate of the O_3 photochemical production at the 685-mbar model level over the United States (see Figure 1), which in turn suggests that the model-generated NO_x mixing ratios at this altitude are perhaps too high in this region (see Appendix).

3.2. Comparisons With Measurements at Maritime Locations

Multiple-year measurements of surface O_3 at Sable Island (44°N, 60°W) [*Parrish et al.*, 1993; D. D. Parrish, private communication] and Bermuda (32°N, 65°W) [*Oltmans and Levy*, 1992; S. J. Oltmans, private communication] provide an excellent opportunity to evaluate model performance over two distinct regions of the NAO. A shorter record of surface O_3 measurements is also available in the eastern NAO at the Azores (39°N, 27°W) (S. J. Oltmans, private communication). The statistics of the modeled summertime surface O_3 time series at these three sites are compared to observations in Figure 4. At Sable Island and Bermuda the modeled O_3 levels are within a few parts per billion by volume of the observations over the entire range of the data. In particular, the modeled means and medians at both sites are almost identical to the observed means and medians. At the Azores site, the modeled O_3 is significantly lower than the measurements. This disagreement may be the result of an underestimate of the transport efficiency of either stratospheric or anthropogenic O_3 to the eastern NAO, or due to excessive photochemical O_3 destruction during transport to this region in the model. It should be noted, however, that the observed statistics are less well defined from a climatological perspective at the Azores since the observations only span one summer.

Vertical profiles of ozone mixing ratios have also been measured at Bermuda and the Azores during the North Atlantic Regional Experiment (NARE) intensive in the summer of 1993 (S. J. Oltmans, private communication). In all, about 23 profiles, with a vertical resolution of 1 km, are available at each

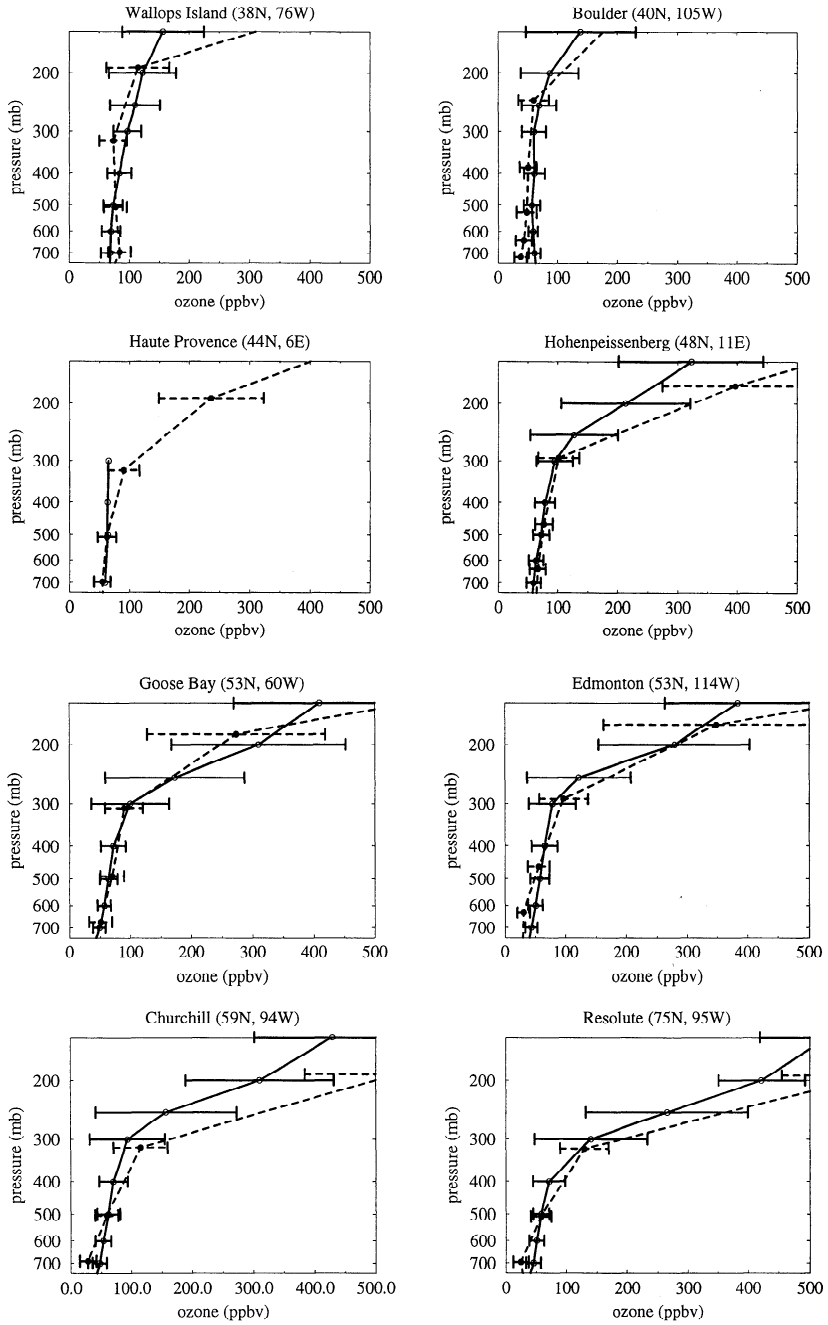

Figure 3. Comparison of modeled July–August mean vertical O_3 profiles in the free troposphere with observations from North America and Europe. Observed means are shown connected by vertical solid lines. Modeled means are shown connected by vertical dashed lines. Horizontal solid lines show the standard deviations for the observed data, and dashed horizontal lines show the simulated standard deviations.

site. Given the sparsity of the data record, we choose to compare the vertical profile of the mean O_3 measured at each altitude with the corresponding model results (see Figure 5). At Bermuda the modeled vertical O_3 profile, in the boundary layer below 2 km and in the free troposphere above 5 km, is in reasonably good agreement with the measurements. However, the model overestimates the amount of O_3 in the lower free troposphere and thus does not capture the observed steep gradient between 3 and 5 km at this site. At the Azores site, modeled free-tropospheric O_3 mixing ratios agree quite well with the observations, though the surface to upper troposphere gradient is too high in the model due to the underestimate of boundary layer mixing ratios (as discussed in the previous paragraph). The model is unable to simulate the tropospheric O_3 distribution above 8 km at this site since the local mean-tropopause height in the model is too low.

At maritime sites off the coast of Canada a strong positive correlation has been observed between CO and O_3 during summer (see Figure 6). *Parrish et al.* [1993] suggested that the occurrence of elevated levels of O_3 associated with high levels of CO at these sites is due to the transport of photochemically generated O_3 from North America out over the NAO. These observed CO-O_3 correlations therefore provide a test of the model's ability to transport polluted continental boundary

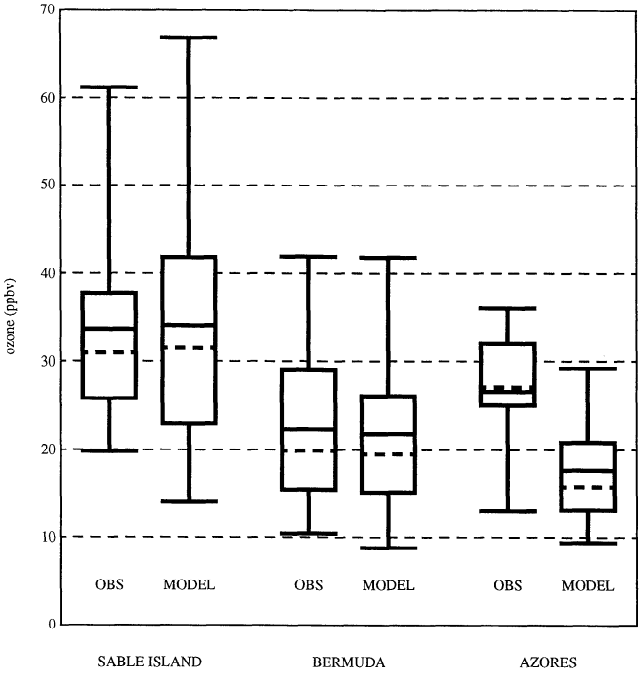

Figure 4. Box and whisker plots of the 5th, 25th, 75th, and 95th percentiles of observed and modeled July–August-mean surface O_3 mixing ratios at three sites in the North Atlantic Ocean. Means and medians at each site are denoted by solid and dashed lines, respectively, in rectangles. The observations cover the time periods 1991–1993 at Sable Island (D. D. Parrish, private communication), 1989–1993 at Bermuda (S. J. Oltmans, private communication), and 1993 at the Azores (S. J. Oltmans, private communication).

layer air from North America to the NAO. Using the same GCTM, we have performed an independent simulation of CO. Included in this CO calculation are preliminary estimates of the emissions of CO from fossil-fuel combustion and biomass- and wood fuel-burning sources as well as the source of CO due to oxidation of methane. In addition, the CO source from oxidation of isoprene and monoterpenes is calculated using spatially and temporally varying maps of isoprene and monoterpene fluxes [*Guenther et al.*, 1995], along with effective oxidation yields of 2.5 molecules of CO/molecule for isoprene [*Miyoshi et al.*, 1994] and 0.8 molecules of CO/molecule for monoterpenes (R. D. Saylor, private communication).

In Figure 6 the relationship between the modeled CO and the O_3 at Sable Island is compared to observations. Despite the limited number of model data points relative to the observations, the model succeeds in reproducing the main feature in the observations; that is, at this site, there is a general trend of higher O_3 levels associated with elevated CO levels. A linear regression between the modeled O_3 and the CO yields a slope of 0.28 ($r^2 = 0.75$), which is in excellent agreement with the observed CO-O_3 relationship (slope = 0.27, $r^2 = 0.6$) at this site. We emphasize that our CO calculation is only exploratory in nature, and a more detailed analysis of the CO-O_3 correlations at this site as well as at other sites in the NAO will be undertaken after further refinements to the CO simulation in the model.

3.3. Simulated Three-Dimensional O_3 Distribution Over the NAO

In the previous two subsections we have evaluated the performance of our model by comparing simulated O_3 mixing ratios to observations at a variety of locations and altitudes. Despite some apparent deficiencies the model reproduces important characteristics of summertime O_3 measurements over the NAO and adjacent continents. This suggests that the basic large-scale features of tropospheric photochemistry and transport, which together control the summertime distribution of tropospheric O_3 over the NAO, are adequately simulated by the model. We now present a three-dimensional picture of the mean summertime O_3 distribution simulated by the model over the extratropical NAO and the adjacent continents (Figure 7).

In the boundary layer the modeled mean O_3 mixing ratios range from greater than 60 ppbv over industrial regions in North America and Europe (where NO_x emissions are high) to less than 20 ppbv over the central NAO in the subtropics. The influence of North American outflow is seen in a broadband extending northeastward from the East Coast of North America, while outflow from Europe affects a broad region between 30°N and 55°N in the eastern NAO. In the continental outflow region over the western NAO, O_3 mixing ratios range from >50 ppbv near the coast to ~30 ppbv a few thousand kilometers downwind from the North American industrial regions.

At the 685- and 500-mbar model levels the highest O_3 levels occur over the south central and southeastern United States. A more detailed analysis shows that a large fraction (50% or greater) of the O_3 in this region is due to chemical production in the free troposphere, as opposed to upward transport from the continental boundary layer. Thus the higher free-tropospheric O_3 levels over the eastern United States, relative to Europe, are due to the difference in free-tropospheric O_3 photochemical production rates between these two regions (see Figure 1). There is a relatively strong free-tropospheric source of NO_x from lightning over the south central and southeastern United States in our model, which contributes significantly to in situ O_3 photochemical production in this region (see Appendix). It is likely that this is an artifact in our model, as sonde data from Palestine, Texas, show O_3 values of around 62 ppbv at these altitudes (J. A. Logan, private communication).

Broadbands of relatively high O_3 are also seen stretching in a northeasterly direction over the western and central NAO at

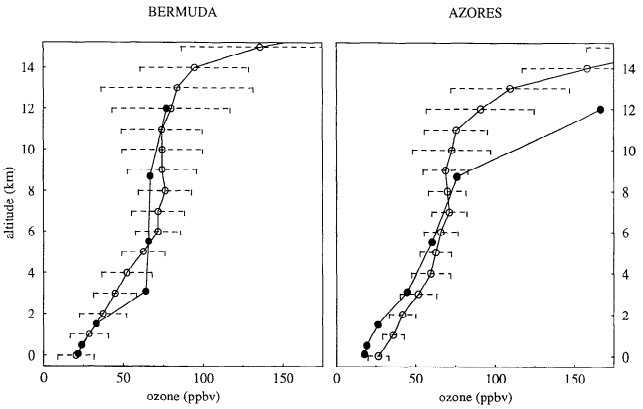

Figure 5. Observed and modeled July–August-mean vertical O_3 profiles at Bermuda and the Azores. Observations are denoted by open circles, and model results are denoted by solid circles. Dashed lines show the standard deviation at each altitude in the observed data. The observed statistics are derived from ozonesonde measurements during July–August 1993 (S. J. Oltmans, private communication).

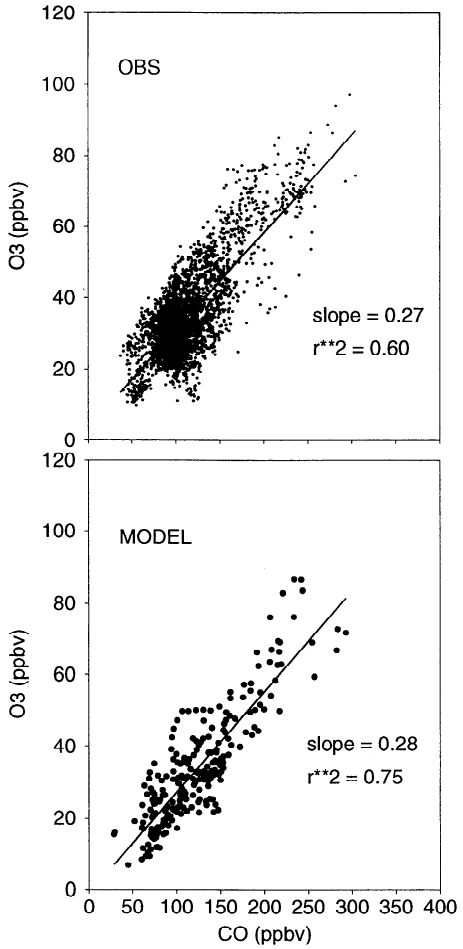

Figure 6. Observed and modeled July–August-mean CO-O_3 relationships at Sable Island. The observations are hourly averages of measurements taken during 1991–1993 (D. D. Parrish, private communication).

the 685- and 500-mbar model levels. This banded structure is absent at the 315-mbar model level, where the simulated O_3 fields have a more zonal character. At this altitude, O_3 levels increase from ~60 ppbv at 30°N to >80 ppbv north of 45°N. The higher levels of O_3 in the free troposphere relative to the boundary layer seen in the vertical profile data from Bermuda and the Azores (see Figure 5) are found to be characteristic of the entire extratropical NAO, and modeled 500-mbar mixing ratios over the whole basin are comparable to O_3 levels in the polluted continental boundary layer.

The geographical patterns in the modeled O_3 distribution also suggest that photochemical production of O_3 over continents, followed by transport, has a widespread impact on O_3 over a large portion of the NAO. The modeled summer-mean tropospheric O_3 distribution over the NAO is therefore the result of a complex interaction between various processes such as transport of photochemically produced O_3 from the continental boundary layer and free troposphere to the NAO, O_3 photochemistry over the NAO itself, and downward transport of "natural" O_3 from the stratosphere.

3.4. Effect of Anthropogenic NO_x Emissions on O_3 Over the NAO

We now use the model to address a key question, namely, to what extent have anthropogenic activities perturbed the summertime O_3 distribution over the NAO? To shed light on this issue, we have performed a second model simulation which is identical to the model simulation described in section 2, except that the mixing ratios and chemical conversion rates of NO_x used in the O_3 photochemical calculations are now taken from a preindustrial NO_x calculation (see Appendix). This scenario is only an approximation of true preindustrial conditions, since potential changes in mixing ratios of related species such as CO, methane, and OH have been neglected in our calculations. The yield of O_3 molecules per NO_x molecule oxidized is still assumed to be 8.5. In reality this is probably higher because of the nonlinear dependence of the O_3 production rate on the ambient NO_x concentration. However, we have performed a sensitivity calculation using a yield of 20 and find that the simulated preindustrial O_3 mixing ratios over the NAO are quite insensitive to this change.

The impact of anthropogenic NO_x emissions can be assessed by comparing the simulated preindustrial tropospheric O_3 distribution to the modeled present-day distribution discussed in the previous sections. While both the preindustrial and present-day calculations are uncertain to some degree, our model results strongly suggest that anthropogenic NO_x emissions have substantially increased O_3 concentrations in much of the troposphere above the NAO. The difference between model-calculated present-day and preindustrial O_3 levels is shown in Figure 8. In the boundary layer and lower free troposphere the largest increases are seen in the industrialized regions of the United States and Europe, where present-day O_3 levels are calculated to be 30–50 ppbv higher than corresponding preindustrial O_3 levels. In the middle and upper free troposphere the calculated changes are largest between 40°N and 50°N downwind of North America and between 45°N and 55°N over Europe. Our calculations show anthropogenic activities have substantially altered O_3 levels throughout the troposphere over the extratropical NAO and that modeled present-day O_3 levels are at least 15–30 ppbv higher than corresponding preindustrial levels even over the central NAO.

An alternative perspective of this impact may be gained by examining Figure 9, which shows the ratio of model-calculated present-day and preindustrial O_3 concentrations. Below 3 km the modeled present-day O_3 levels are at least twice as high as corresponding preindustrial O_3 over the entire extratropical NAO. At these altitudes the modeled change in O_3 levels is particularly striking north of 40°N, where present-day O_3 levels are 2.5–3 times higher than preindustrial levels even at locations farthest away from the continental boundaries. The calculated anthropogenic impact is smaller at the 500-mbar model level than at lower altitudes but is still substantial, with calculated present-day O_3 levels at least 50% higher than preindustrial levels over the entire extratropical NAO. Our model results suggest that the influence of anthropogenic emissions is felt in the upper troposphere as well. For example, at the 315-mbar model level, simulated present-day O_3 levels are 20–40% higher than corresponding preindustrial levels. However, we qualify this conclusion by noting that our present-day model results are perhaps most uncertain in the upper troposphere (see section 3.1).

It is interesting to note that at or below 500 mbar the calculated relative change in O_3 from preindustrial to present is smaller over the United States than over Europe. This is a reflection of the fact that modeled preindustrial O_3 levels are somewhat higher over the United States compared to Europe. In fact, the relative change between present-day and preindus-

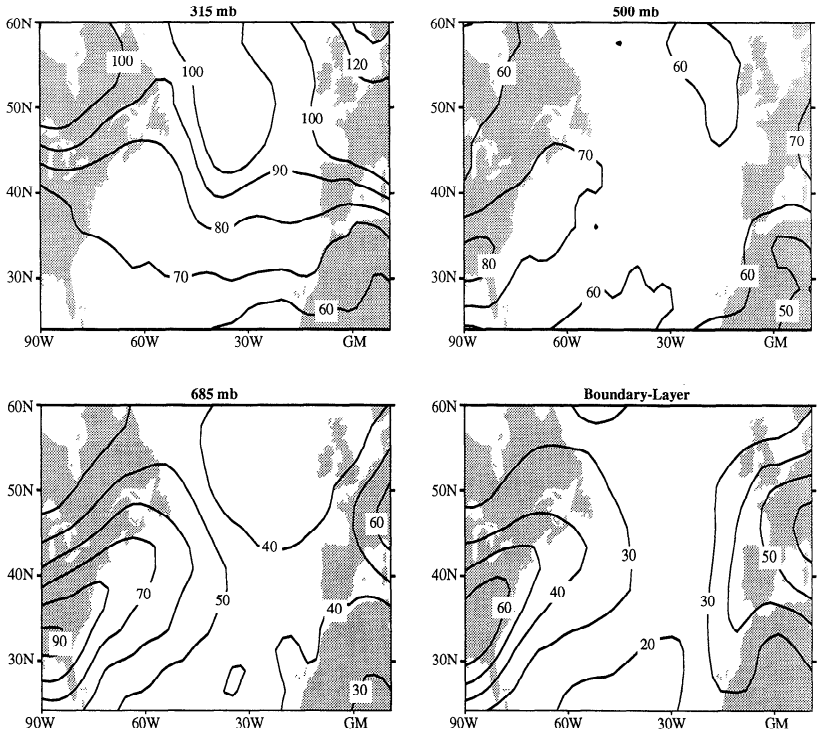

Figure 7. Model-simulated July–August-mean boundary layer and free-tropospheric O_3 mixing ratios. Contour levels are 20, 30, 40, 50, 60, 70, 80, 90, 100, 120, and 140 ppbv O_3.

trial O_3 at the 685-mbar model level is higher over the NAO north of 40°N than it is over the United States, despite the fact that the absolute change in O_3 levels is larger over the latter region (see Figure 8).

A comparison of our model results with the *Crutzen and Zimmerman* [1991] model is difficult since only surface and zonal-average maps are presented in their paper. Their calculations overestimate present-day O_3 over the NAO, but their ratio of preindustrial to present-day surface O_3 appears to be similar to our estimate. It is also worth noting that our calculated preindustrial boundary layer O_3 levels over western Europe of 10–20 ppbv are qualitatively consistent with the *Volz and Kley* [1988] estimate of preindustrial summertime surface O_3 concentrations at Montsouris.

Summary

We have developed and implemented a three-dimensional GCTM with a simplified representation of tropospheric photochemistry to simulate the summertime O_3 distribution over the NAO. Results from this model have been compared to both surface and free-tropospheric O_3 observations at various locations and during time periods relevant to this study. The model reproduces the major features in these observations, though some shortcomings are evident. These include an underestimate of boundary layer O_3 over the eastern NAO, an overestimate of lower free-tropospheric O_3 over the western NAO, and difficulty in reproducing the upper tropospheric ozonesonde measurements over North America. Nevertheless, the model results offer useful insights into the behavior of tropospheric O_3 over the NAO. We see that geographically varying patterns of O_3 photochemical production and destruction, both in the boundary layer and in the free troposphere, interact with transport processes to determine the three-dimensional O_3 distribution over the NAO.

In addition to providing a three-dimensional view of tropospheric O_3, a significant facet of our study is the calculated large-scale impact of anthropogenic NO_x emissions on summertime O_3 over the NAO. While this is significant from an atmospheric chemistry perspective, perturbations of the magnitude and spatial extent indicated by our simulations may have a profound effect on the climate system as well, since O_3 is a key player in determining the rate at which greenhouse gases such as methane are removed from the atmosphere. Our study therefore highlights the fact that an important component of global change may be the impact of anthropogenic NO_x emissions on global tropospheric chemistry and climate. The next step, from our modeling perspective, will be to extend the GCTM described here to be applicable to other geographical regions and seasons, in order to obtain further insights into the factors shaping the global tropospheric O_3 distribution.

Appendix

The GFDL GCTM used in this study has been previously applied to simulate the present-day global distribution of NO_y compounds. The simulated three-dimensional NO_x fields from this calculation have been used to calculate O_3 photochemistry for present-day conditions, as described in section 2. We have also previously simulated the preindustrial NO_y distribution, and the NO_x fields from this calculation have been used in the preindustrial O_3 simulation, as described in section 3.5). Global aspects of some components of the NO_y simulations have been described by *Kasibhatla et al.* [1991, 1993], *Levy et al.* [1991, 1993, 1995], *Kasibhatla* [1993], *Galloway et al.* [1994], and *Moxim et al.* [1995], and a more comprehensive description

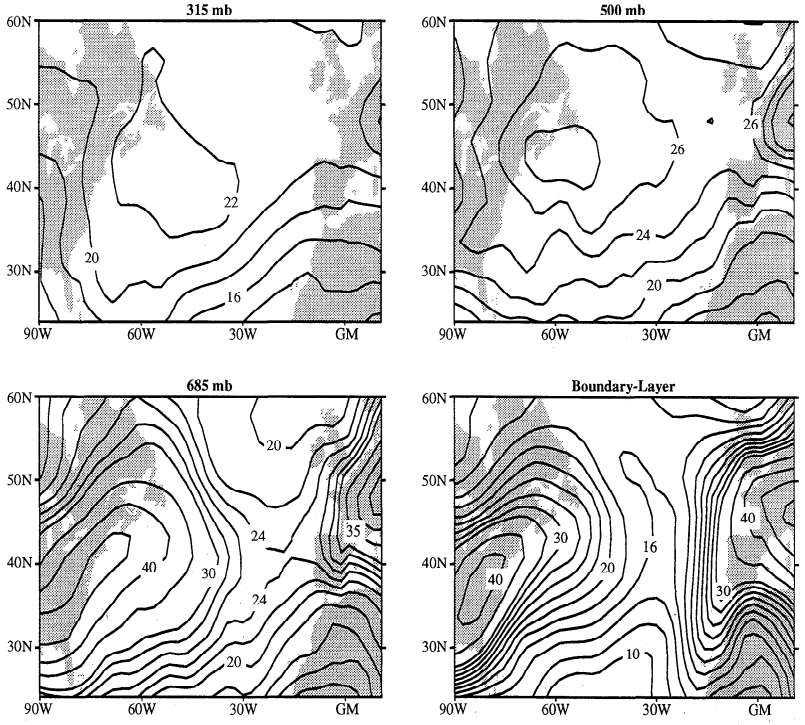

Figure 8. Difference between modeled present-day and preindustrial July–August-mean boundary layer and free-tropospheric O_3 mixing ratios. Contour levels are 10, 12, 14, 16, 18, 20, 22, 24, 26, 28, 30, 35, 40, 45, and 50 ppbv O_3.

and analysis of these simulations will be the subject of a future paper. In this section we present salient features of the calculated summertime NO_x distribution over North America, parts of Europe, and the NAO.

Sources of NO_x from both anthropogenic and natural sources are included in the present-day NO_y simulation. These include fossil-fuel combustion emissions near the surface [*Levy and Moxim*, 1989], biomass- and wood fuel-burning emissions

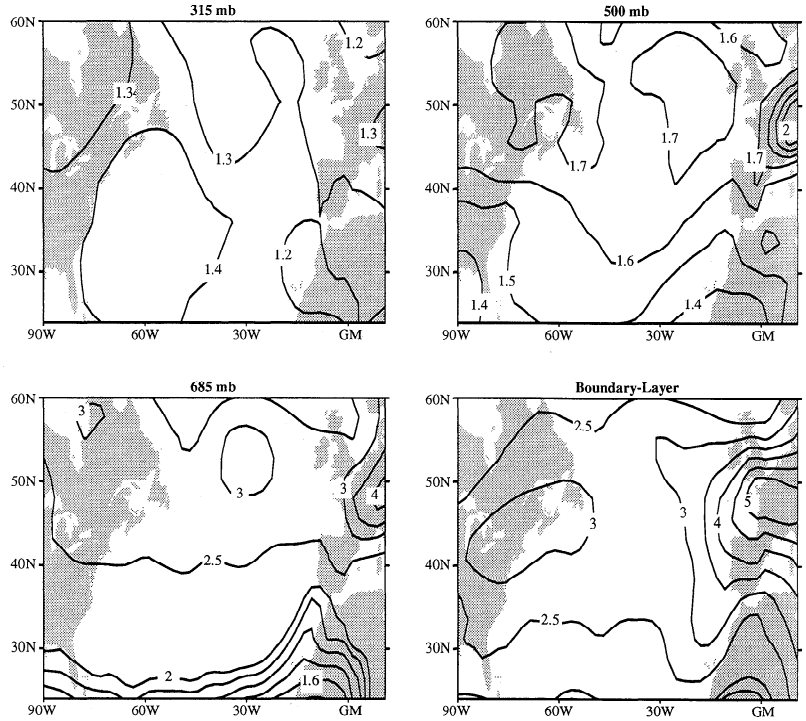

Figure 9. Ratio of modeled July–August-mean boundary layer and free-tropospheric O_3 mixing ratios for present-day conditions relative to corresponding preindustrial O_3 levels. Contour levels are 1.2, 1.3, 1.4, 1.5, 1.6, 1.7, 1.8, 1.9, 2, 2.5, 3, 3.5, 4, 4.5, and 5.

[*Levy et al.*, 1991], nitrogen fixation by lightning [*Levy et al.*, 1995], natural and fertilizer-induced biogenic emissions from soils [*Yienger and Levy*, 1995], emissions from subsonic aircraft [*Kasibhatla*, 1993], and production by oxidation of nitrous oxide in the stratosphere [*Kasibhatla et al.*, 1991]. The model explicitly treats the transport, chemistry, and removal of NO_x, HNO_3, and peroxyacetyl nitrate (PAN). The parameterized gas phase chemical scheme described by *Kasibhatla et al.* [1993], along with a parameterization to take into account the heterogeneous nighttime formation of HNO_3 by oxidation of nitrogen pentoxide, is used in these calculations. In the gas phase chemical calculations, specified two-dimensional, monthly mean OH fields are used to calculate the chemical conversion of NO_x to HNO_3 [*Kasibhatla et al.*, 1993]. Fossil-fuel combustion emissions from surface-based and aircraft sources and fertilizer-induced biogenic emissions are excluded in the preindustrial NO_y simulation. In the context of this study, it should be noted that the OH fields used in the preindustrial NO_y simulation are the same as those used in the present-day NO_y simulation.

The model-simulated, June–July–August mean NO_x distributions over North America and the NAO for the present-day and preindustrial scenarios are shown in Figures 10 and 11, respectively. The simulated present-day boundary layer NO_x concentrations are highest (ranging from 1 to 2 ppbv) in the industrialized regions of North America and Europe and decrease rapidly with increasing distance from these source regions because of the relatively short lifetime of NO_x in the lower troposphere. Over the continental source regions the simulated present-day NO_x concentrations at the 685-mbar model level are about 4–5 times lower than in the boundary layer, while NO_x concentrations in the middle and upper troposphere are about 5–10 times lower than corresponding boundary layer concentrations.

As expected, the simulated preindustrial boundary layer NO_x concentrations in the industrialized regions are substantially smaller than corresponding present-day levels. However, the difference between the simulated present-day and preindustrial NO_x concentrations is much smaller in the free troposphere over the south central and southeastern United States, due to the presence of a relatively strong lightning source in this region of our model. This is also the reason why calculated present-day free-tropospheric NO_x concentrations over this region are significantly higher than over Europe. This is even more clearly evident in Figure 11, where the simulated free-tropospheric preindustrial NO_x concentrations exhibit a significant peak centered at about 90°W between 30°N and 35°N.

The modeled summertime free-tropospheric NO_x distribution is in reasonable agreement with measurements from a few selected airborne field campaigns. For example, mean NO_x mixing ratios of 48 and 43 pptv over the Hudson Bay lowlands and over northern Labrador/Quebec, respectively, were observed in the free troposphere during the Arctic Boundary Layer Expedition (ABLE) 3B mission in the summer of 1990 [*Sandholm et al.*, 1994]. In the Hudson Bay lowlands region the simulated July-mean NO_x mixing ratio ranges from 40 to 55 pptv at 500 mbar, in good agreement with the observations. In the northern Labrador region the simulated 500-mbar July-mean NO_x mixing ratio is 30–35 pptv, which is slightly lower than the observed value. Over Alaska the mean observed free-tropospheric NO_x mixing ratio was 31 pptv during the ABLE 3A mission in the summer of 1988 [*Sandholm et al.*, 1994], while the modeled 500-mbar July-mean NO_x mixing ratio in this region ranges from 18 to 24 pptv. Measurements off the eastern coast of North America between 40°N and 50°N during the south bound leg of the Stratospheric Ozone (STRATOZ) III experiment show mean NO mixing ratios ranging from 12 to 17 pptv between 5.5 and 6.5 km and between 47 and 86 pptv

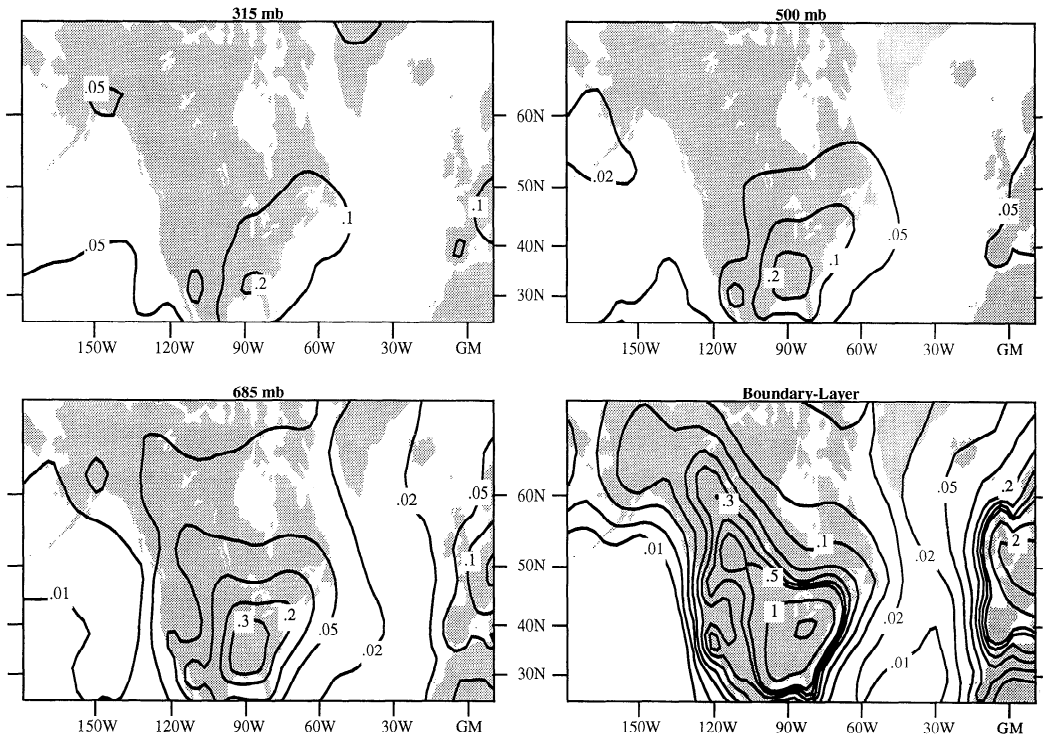

Figure 10. Model-simulated June–July–August-mean boundary layer and free-tropospheric NO_x mixing ratios for present-day NO_x emissions. Contour levels are 0.01, 0.02, 0.05, 0.1, 0.2, 0.3, 0.4, 0.5, 1, and 2 ppbv NO_x.

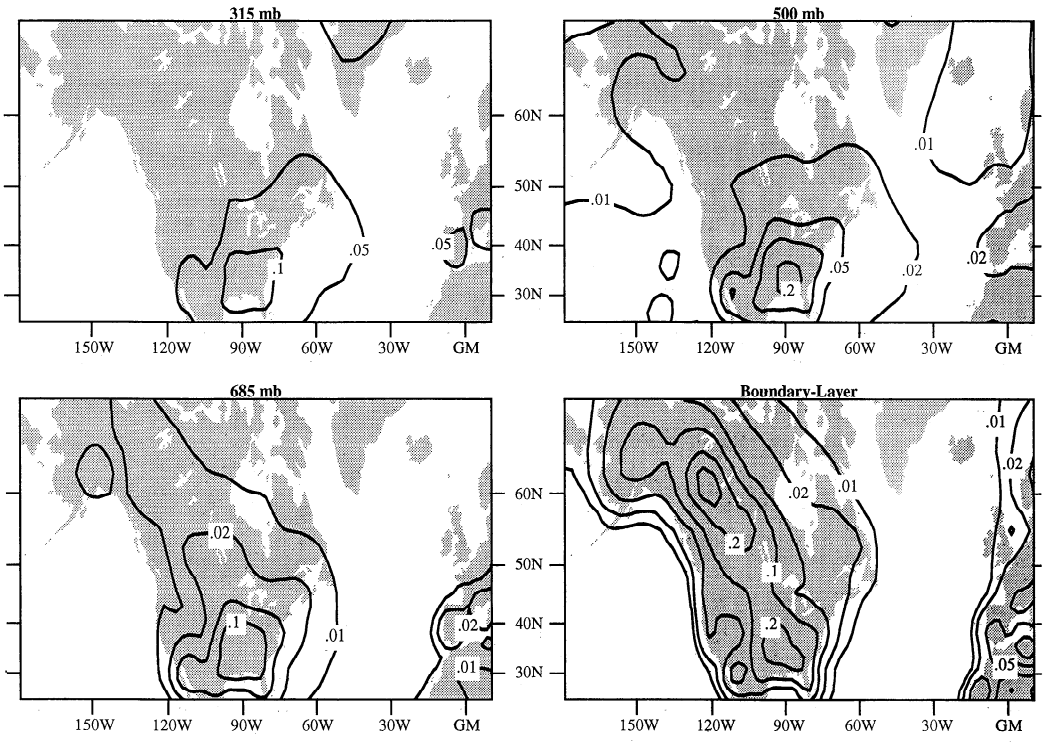

Figure 11. Model-simulated June–July–August-mean boundary layer and free-tropospheric NO_x mixing ratios for preindustrial NO_x emissions. Contour levels are 0.01, 0.02, 0.05, 0.1, 0.2, and 0.3 ppbv NO_x.

between 8.5 and 9.5 km [*Drummond et al.*, 1998]. The corresponding NO mixing ratios inferred from the June-mean modeled NO_x mixing ratios in this region range from 27 to 37 pptv at the 500-mbar model level and from 53 to 82 pptv at the 315-mbar model level. While the model appears to be in good agreement with the upper tropospheric measurements and high compared to the midtropospheric measurements, it should be noted that the extremely limited number of measurements in this region during the STRATOZ III experiment precludes a more rigorous evaluation of the model results.

Acknowledgments. We thank J. A. Logan for providing ozonesonde data at North American sites, S. J. Oltmans for providing ozone measurements from Bermuda and the Azores, and D. D. Parrish for providing carbon monoxide and ozone measurements at Sable Island. We are especially grateful to D. J. Jacob, J. A. Logan, J. D. Mahlman, W. J. Moxim, L. M. Perliski, and an anonymous reviewer for their thoughtful comments on the original draft of this manuscript. This research was partly funded by the Atmospheric Chemistry Project of the NOAA Climate and Global Change Program under grant NA36GP0250 and the National Science Foundation under grant ATM-9213643.

References

Altshuller, A. P., Association of oxidant episodes with warm stagnating anticyclones, *J. Air. Pollut. Control Assoc.*, *28*, 152–155, 1978.

Beekmann, M., G. Ancellet, and G. Megie, Climatology of tropospheric ozone in southern Europe and its relation to potential vorticity, *J. Geophys. Res.*, *99*, 12,841–12,853, 1994.

Brost, R. A., R. B. Chatfield, J. P. Greenberg, P. L. Haagenson, B. G. Heikes, S. Madronich, B. A. Ridley, and P. R. Zimmerman, Three-dimensional modeling of transport of chemical species from continents to the Atlantic Ocean, *Tellus*, *40B*, 358–379, 1988.

Chameides, W., and J. C. G. Walker, A photochemical theory of tropospheric ozone, *J. Geophys. Res.*, *78*, 8751–8760, 1973.

Chameides, W. L., et al., Ozone precursor relationships in the ambient atmosphere, *J. Geophys. Res.*, *97*, 6037–6055, 1992.

Chatfield, R., and H. Harrison, Tropospheric ozone, 2, Variations along a meridional band, *J. Geophys. Res.*, *82*, 5969–5976, 1977.

Chin, M., D. J. Jacob, J. W. Munger, D. D. Parrish, and B. G. Doddridge, Relationship of ozone and carbon monoxide over North America, *J. Geophys. Res.*, *99*, 14,565–14,573, 1994.

Crutzen, P. J., Photochemical reaction initiated by and influencing ozone in unpolluted tropospheric air, *Tellus*, *26*, 58–70, 1974.

Crutzen, P. J., and L. T. Gidel, A two-dimensional model of the atmosphere, 2, The tropospheric budgets of the anthropogenic chlorocarbons, CO, CH_4, CH_3Cl, and the effects of various NO_x sources on tropospheric ozone, *J. Geophys. Res.*, *88*, 6641–6661, 1983.

Crutzen, P. J., and P. H. Zimmerman, The changing photochemistry of the troposphere, *Tellus*, *43AB*, 136–151, 1991.

Drummond, J. W., D. H. Ehhalt, and A. Volz, Measurements of nitric oxide between 0 and 12 km altitude and 67°N to 60°S latitude obtained during STRATOZ III, *J. Geophys. Res.*, *93*, 15,831–15,849, 1988.

Fishman, J., C. E. Watson, J. C. Larsen, and J. A. Logan, Distribution of tropospheric ozone determined from satellite data, *J. Geophys. Res.*, *95*, 3599–3617, 1990.

Galloway, J. N., H. Levy II, and P. S. Kasibhatla, Year 2020: Consequences of population growth and development on deposition of oxidized nitrogen, *Ambio*, *23*, 120–123, 1994.

Guenther, A., et al., A global model of natural volatile organic compound emissions, *J. Geophys. Res.*, *100*, 8873–8892, 1995.

Harriss, R. C., E. V. Browell, D. I. Sebacher, G. L. Gregory, R. R. Hinton, S. M. Beck, D. S. McDougal, and S. T. Shipley, Atmospheric transport of pollutants from North America to the North Atlantic Ocean, *Nature*, *308*, 722–724, 1984.

Hough, A. M., and R. G. Derwent, Changes in the global concentration of tropospheric ozone due to human activities, *Nature*, *344*, 645–648, 1990.

Isaksen, I. S. A., and Ø. Hov, Calculations of trends in the tropospheric concentrations of O_3, OH, CO, CH_4, and NO_x, *Tellus*, *39B*, 271–285, 1987.

Jacob, D. J., et al., Simulation of summertime ozone over North America, *J. Geophys. Res.*, *98*, 14,797–14,816, 1993a.

Jacob, D. J., et al., Factors regulating ozone over the United States and its export to the global atmosphere, *J. Geophys. Res.*, *98*, 14,817–14,826, 1993b.

Junge, C. E., Global ozone budget and exchange between stratosphere and troposphere, *Tellus*, *14*, 363–377, 1962.

Kasibhatla, P. S., NO_y from sub-sonic aircraft emissions: A global three-dimensional model study, *Geophys. Res. Lett.*, *20*, 1707–1710, 1993.

Kasibhatla, P. S., H. Levy II, W. J. Moxim, and W. L. Chameides, The relative impact of stratospheric photochemical production on tropospheric NO_y levels: A model study, *J. Geophys. Res.*, *96*, 18,631–18,646, 1991.

Kasibhatla, P. S., H. Levy II, and W. J. Moxim, Global NO_x, HNO_3, PAN, and NO_y distributions from fossil fuel combustion emissions: A model study, *J. Geophys. Res.*, *98*, 7165–7180, 1993.

Law, K. S., and J. A. Pyle, Modeling the response of tropospheric trace species to changing source gas concentrations, *Atmos. Environ.*, *25A*, 1863–1871, 1991.

Levy, H., II, Normal atmosphere: Large radical and formaldehyde concentrations predicted, *Science*, *173*, 141–143, 1971.

Levy, H., II, and W. J. Moxim, Simulated global distribution and deposition of reactive nitrogen emitted by fossil fuel combustion, *Tellus*, *41*, 256–271, 1989.

Levy, H., II, J. D. Mahlman, and W. J. Moxim, Tropospheric N_2O variability, *J. Geophys. Res.*, *87*, 3061–3080, 1982.

Levy, H., II, J. D. Mahlman, W. J. Moxim, and S. C. Liu, Tropospheric ozone: The role of transport, *J. Geophys. Res.*, *90*, 3753–3772, 1985.

Levy, H., II, W. J. Moxim, P. S. Kasibhatla, and J. A. Logan, The global impact of biomass burning on tropospheric reactive nitrogen, in *Global Biomass Burning: Atmospheric, Climatic, and Biospheric Implications*, pp. 363–369, edited by J. S. Levine, The MIT Press, Cambridge, Mass., 1991.

Levy, H., II, W. J. Moxim, and P. S. Kasibhatla, Impact of global NO_x sources on the northern latitudes, in *NATO ASI Series*, vol. 17, *The Tropospheric Chemistry of Ozone in Polar Regions*, edited by H. Niki and K. H. Becker, pp. 77–88, Springer-Verlag, New York, 1993.

Levy, H., II, W. J. Moxim, and P. S. Kasibhatla, A global three-dimensional time-dependent lightning source of tropospheric NO_x, *J. Geophys. Res.*, in press, 1995.

Lin, X., M. Trainer, and S. C. Liu, On the nonlinearity of the tropospheric ozone production, *J. Geophys. Res.*, *93*, 15,879–15,888, 1988.

Liu, S. C., M. Trainer, F. C. Fehsenfeld, D. D. Parrish, E. J. Williams, D. W. Fahey, G. Hübler, and P. C. Murphy, Ozone production in the rural troposphere and the implications for regional and global ozone distributions, *J. Geophys. Res.*, *92*, 4191–4207, 1987.

Logan, J. A., Trends in the vertical distribution of ozone: An analysis of ozonesonde data, *J. Geophys. Res.*, *99*, 25,553–25,585, 1994.

Lu, Y., and M. A. K. Khalil, Tropospheric OH: Model calculations of spatial, temporal, and secular variations, *Chemosphere*, *23*, 397–444, 1991.

Mahlman, J. D., and W. J. Moxim, Tracer simulations using a global general circulation model: Results from a midlatitude instantaneous source experiment, *J. Atmos. Sci.*, *35*, 1340–1374, 1978.

Mahlman, J. D., H. Levy II, and W. J. Moxim, Three-dimensional tracer structure and behavior as simulated in two ozone precursor experiments, *J. Atmos. Sci.*, *37*, 655–685, 1980.

Manabe, S., and J. L. Holloway Jr., The seasonal variation of the hydrologic cycle as simulated by a global model of the atmosphere, *J. Geophys. Res.*, *80*, 1617–1649, 1975.

Manabe, S., and R. F. Strickler, Thermal equilibrium of the atmosphere with a convective adjustment, *J. Atmos. Sci.*, *21*, 361–385, 1964.

Manabe, S., and R. T. Wetherald, Thermal equilibrium of the atmosphere with a given distribution of relative humidity, *J. Atmos. Sci.*, *24*, 241–259, 1967.

Manabe, S., D. G. Hahn, and J. L. Holloway, Jr., The seasonal variation of the tropical circulation as simulated by a global model of the atmosphere, *J. Atmos. Sci.*, *31*, 43–83, 1974.

Mathews, E., Global vegetation and land use: New high-resolution data bases for climate studies, *J. Clim. Appl. Meteorol.*, *22*, 474–487, 1983.

Mathur, R., K. L. Schere, and A. Nathan, Dependencies and sensitivity of tropospheric oxidants to precursor concentrations over the northeast United States: A model study, *J. Geophys. Res.*, *99*, 10,535–10,552, 1994.

McKeen, S. A., E.-Y. Hsie, M. Trainer, R. Tallamraju, and S. C. Liu, A regional model study of the ozone budget in the eastern United States, *J. Geophys. Res.*, *96*, 10,809–10,845, 1991.

Miyoshi, A., S. Hatakeyama, and N. Washida, OH radical-initiated photooxidation of isoprene: An estimate of global CO production, *J. Geophys. Res.*, *99*, 18,799–18,787, 1994.

Moxim, W. J., Simulated transport of NO_y to Hawaii during August: A synoptic study, *J. Geophys. Res.*, *95*, 5717–5729, 1990.

Nagatani, R. M., A. J. Miller, K. W. Johnson, and M. E. Gelman, An eight-year climatology of meteorological and SBUV ozone data, *NOAA Tech. Rep. NWS 40*, 125 pp., Natl. Weather Serv., Camp Springs, Md., 1988.

Oltmans, S. J., and H. Levy II, Seasonal cycle of surface ozone over the western North Atlantic, *Nature*, *358*, 392–394, 1992.

Oort, A. H., Global atmospheric circulation statistics, 1958–1973, *NOAA Prof. Pap. 14*, 180 pp., U.S. Govt. Print. Off., Washington, D. C., 1983.

Parrish, D. D., J. S. Holloway, M. Trainer, P. C. Murphy, G. L. Forbes, and F. C. Fehsenfeld, Export of North American ozone pollution to the North Atlantic Ocean, *Science*, *259*, 1436–1439, 1993.

Pinto, J. P., and M. A. K. Khalil, The stability of tropospheric OH during ice ages, interglacial epochs and modern times, *Tellus*, *43B*, 136–151, 1991.

Ramanathan, V., R. J. Cicerone, H. B. Singh, and J. T. Kiehl, Trace gas trends and their potential role in climate change, *J. Geophys. Res.*, *90*, 5547–5566, 1985.

Sandholm, S., et al., Summertime partitioning and budget of NO_y compounds in the troposphere over Alaska and Canada: ABLE 3B, *J. Geophys. Res.*, *99*, 1837–1861, 1994.

Thompson, A. M., J. A. Chappellaz, I. Y. Fung, and T. L. Kucsera, The atmospheric CH_4 increase since the Last Glacial Maximum, 2, Interaction with oxidants, *Tellus*, *45B*, 242–257, 1993.

Trainer, M., et al., Correlation of ozone with NO_y in photochemically aged air, *J. Geophys. Res.*, *98*, 2917–2925, 1993.

Volz, A., and D. Kley, Evaluation of the Montsouris series of ozone measurements made in the nineteenth century, *Nature*, *332*, 240–242, 1988.

Volz-Thomas, A., et al., *Proceedings of EUROTRAC Symposium '92*, edited by P. M. Borrell, SPB Acad., The Hague, 1993.

Wang, T., Atmospheric reactive nitrogen oxides and their relationship with urban and rural ozone formation, Ph.D. thesis, Georgia Institute of Technology, Atlanta, 1992.

Wesely, M. L., Parameterization of surface resistances to gaseous dry deposition in regional-scale numerical models, *Atmos. Environ.*, *23*, 1293–1304, 1989.

Wesely, M. L., and B. B. Hicks, Some factors that affect the deposition rates of sulfur dioxide and similar gases on vegetation, *J. Air Pollut. Control Assoc.*, *27*, 110–1116, 1977.

Winkler, P., Surface ozone over the Atlantic Ocean, *J. Atmos. Chem.*, *7*, 73–91, 1988.

World Meteorological Organization (WMO), Scientific assessment of ozone depletion, *WMO Rep. 37*, Global Ozone Res. Monit. Proj., Geneva, 1994.

Yienger, J., and H. Levy II, Empirical model of global soil-biogenic NO_x emissions, *J. Geophys. Res.*, *100*, 11,447–11,464, 1995.

W. L. Chameides, School of Earth and Atmospheric Sciences, Georgia Institute of Technology, Atlanta, GA 30332.

P. Kasibhatla (corresponding author), MCNC, Environmental Programs, Suite 112, 200 Park Office Building, Research Triangle Park, NC 27709.

A. Klonecki, Atmospheric and Ocean Sciences Program, Princeton University, Princeton, NJ 08542.

H. Levy II, NOAA Geophysical Fluid Dynamics Laboratory, Princeton, NJ 08542.

(Received May 3, 1993; revised October 5, 1995;
accepted October 5, 1995.)